DOWN-SCALING OF DRIVE CYCLES FOR EXPERIMENTAL DRIVE CYCLE ANALYSES

Pawan K Dhakal[1] Kourosh Heidarikani[1], Annette Muetze[1]*

[1]*Electric Drives and Machines Institute, Graz University of Technology, Graz, Austria*
**E-mail: pawan.dhakal@tugraz.at*

Keywords: ELECTRIC VEHICLES, DOWN-SCALING, DRIVE CYCLE ANALYSIS, PERFORMANCE MAPS, TRACTION MOTORS

Abstract

Modern electric machines operate within a wide range of torque-speed operating points. Real drive cycles of a real vehicle cannot be tested in the given lab with machines that have smaller ranges and thus the drive cycles need to be down-scaled. To allow for experimental investigations of such driving scenarios even in small laboratory scale analyses, this paper presents a method of down-scaling the drive cycles of different vehicles. Three test case speed-over-time drive cycles are chosen and analysed with two different electric vehicles to derive the corresponding torque-speed profiles for the study. These drive cycles are down-scaled to fit the ratings of the two laboratory test case motors. The down-scaling method aims to replicate the torque-speed characteristics of the original driving cycle while considering the specific characteristics of the motors being used in the laboratory. The effectiveness of the proposed down-scaling method is demonstrated.

1 Introduction

Environmental issues and energy efficiency are some of the major concerning aspects in the modern transportation sector. To increase the energy efficiency and reduce the greenhouse gas emissions, electrification of vehicular powertrains is widely considered as a viable mean [1]. Designing electric machines for these powertrains means balancing the factors such as material usage, cost, and performance with energy conversion efficiency being a crucial one [2], [3]. Standardized driving cycles like Worldwide Harmonized Light Vehicle Test Procedure (WLTP), Federal Test Procedure (FTP), and New European Driving Cycle (NEDC) are used to compare the vehicle performance based on emission and fuel consumption requirements [4], [5]. Each driving cycle consist of vehicle speed over time. For a given drive cycle, the torque that is required to drive the vehicle is determined through a vehicle mechanical model. A simple quasi-static longitudinal vehicle model (QSS) as presented in [6] and also mentioned in [7], [8] can be used.

To analyze a specific drive cycle, a torque-speed profile can be simulated using electromagnetic and/or combined electromagnetic-thermal models. Several approaches for design optimization of electric machines over drive cycles have been presented [9]-[13]. The accuracy of the drive performance or energy conversion efficiency largely depends on the chosen model [2], [14]. The drive chosen for a particular application should be able to function at all the required torque-speed operating points within the thermal limits. To evaluate the performance of the drive, it is often necessary to use three-dimensional finite element or more complex hybrid models, and this can be time consuming and demand a huge computational effort. To overcome this, efficiency maps are used which allow predicting the drive performance while reducing computational time and effort [9], [12], [15].

Efficiencies at different operating points can be determined through analytic, numerical, or experimental methods. In model-based approaches, the accuracy of the performance maps depends on the accuracy of the models used [12], [16]–[18]. However, this approach only allows for steady-state examination and does not consider the influence of transient effects. Experimental validation is typically only performed for a few selected points, so it is important to have a high degree of accuracy in all operating points. This requires careful experimental validation of these points, which can be tedious.

It is possible to plot the different operating points that occur within a drive cycle on a drive operating area, and then use performance maps (as look-up tables) to compute the drive performance at these individual operating points. To be able to investigate these operating points and to compare different methods of analysis with the lab machines where expensive high-power and high-speed test benches are usually not an option, this paper presents a methodology to down-scale the real drive cycles of EVs for laboratory testing. In this work, real drive cycles are scaled down to fit the ranges of the lab motors to explore the advantages and the limits of the chosen method to predict the drive efficiency for selected drive cycles. This will allow for the generalization of the findings, extending their applicability to real EV motors. The overall workflow of the study is shown in Fig. 1. Section 2 introduces the longitudinal vehicle model, Section 3 presents the state of art of the proposed down-scaling method, Section 4 details the example cases considered, Section 5 showcases the findings and discussions based on the proposed method and finally Section 6 concludes the paper.

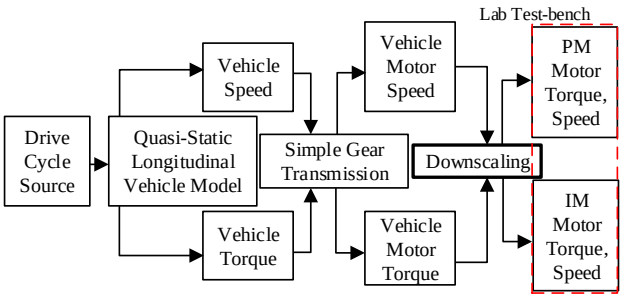

Fig. 1: Workflow of the study.

2 Longitudinal Vehicle Model

An electric vehicle power-train consist of an electric motor and selection of the motor is determined based on the vehicle dynamics and drive cycle that the vehicle operates. To determine the vehicle driving power and energy, understanding of fundamental principles of vehicle mechanics is very important [19]. Fig. 2 shows the different forces acting on a vehicle. The total tractive force of the vehicle is thus given by (1).

$$F_{\text{traction}} = F_{\text{rolling}} + F_{\text{aero}} + F_{\text{grade}} + F_{\text{accel}} \tag{1}$$

The rolling resistance force (F_{rolling}) depends on the rolling resistance coefficient (f_{r}) and for a vehicle of mass (M) and the acceleration due to gravity (g), it is given by (2).

$$F_{\text{rolling}} = Mgf_{\text{r}}\cos(\theta) \tag{2}$$

The aerodynamic drag resistance force (F_{aero}) is proportional to the square of the vehicle's linear speed (v) and depends on the vehicle frontal area (A_{front}), the aerodynamic drag coefficient (C_{d}), and the air density (ρ).

$$F_{\text{aero}} = \frac{1}{2}\rho A_{\text{front}} C_{\text{d}} v^2 \tag{3}$$

The grade resistance force is given by (4).

$$F_{\text{grade}} = Mg\sin(\theta) \tag{4}$$

The acceleration resistive force (F_{accel}) depends on the rotating inertia of the several rotating components present within a vehicle. These rotating elements include pulleys, axles, wheels, bearings etc. The effect of such rotating elements is almost negligible compared to the vehicle mass. For a rotational inertia constant (α), the accelerative resistance force is calculated as in (5).

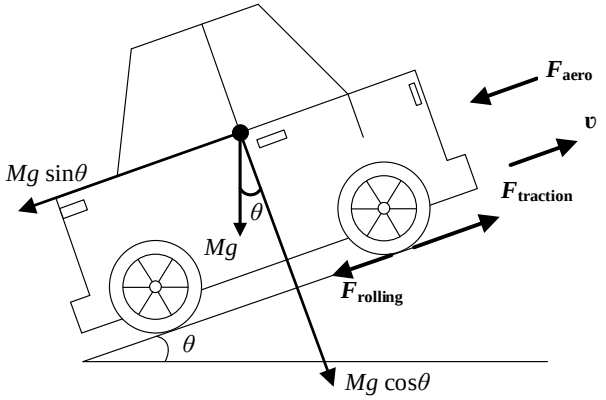

Fig. 2: Forces acting on an EV.

$$F_{\text{accel}} = \alpha Mg\frac{dv}{dt} \tag{5}$$

With calculation of total resistive forces for a given vehicle with known wheel radius (r_{wheel}), the total tractive torque and power on wheel thus can be calculated as in (6) and (7) respectively.

$$T_{\text{wheel}} = F_{\text{traction}} \times r_{\text{wheel}} \tag{6}$$

$$P_{\text{wheel}} = F_{\text{traction}} \times v \tag{7}$$

Now, with this, for a known gear ratio (i) , the torque and the speed of the motor used in the vehicle can be calculated by (8) and (9) respectively. The angular speed of the wheel can be calculated from the linear speed with known wheel radius $(\omega_{\text{wheel}} = \frac{v}{r_{\text{wheel}}})$.

$$T_{\text{motor}} = \frac{T_{\text{wheel}}}{i} \tag{8}$$

$$w_{\text{motor}} = i \times w_{\text{wheel}} \tag{9}$$

3 Proposed Method of Down-Scaling

In this section, the proposed method of down-scaling of drive cycles is illustrated. First, the torque-speed operating points coming out of the QSS model are down-scaled into the dimensionless domain. The drive cycles are then down-scaled to obtain the new torque-speed operating points for the comparison.

3.1 Operating Points

The dimensionless method is used to down-scale the drive cycle operating points. Dimensional analysis has its roots in work by Euler, Newton, Fourier, Maxwell, and Rayleigh and a similar method is formalized as the Dimensionless Pi Theorem by Buckingham and Szirtes [20], [21]. The output of the quasi-static model is altered using the dimensionless variable method based on the selected motor parameters to generate the new torque and speed operating points.

The feasibility of down-scaling is then assessed by examining the steady-state torque-speed characteristics of the motors of the vehicles with respect to the test case motors available in the lab [22].

In the dimensionless method, the variables that need to be scaled down are the torque (T) and the rotational speed (Ω), which are the outputs of the quasi-static model. To implement the method, the number of system parameters $N(T, \Omega)$ and physical dimensions M(length, mass, and time) needed to describe all N parameters are considered. Torque, speed, and power have dimensions of $[\text{m}^2\ \text{kg}\ \text{s}^{-2}]$, $[\text{s}^{-1}]$, and $[\text{m}^2\ \text{kg}\ \text{s}^{-3}]$ respectively in the International System of Units (SI). The parameters $T_{\max}$ and $P_{\max}$ are used to convert between the non-dimensional and the dimensional representations in the motor operating points' down-scale procedure. Three fundamental dimensions (length, mass, and time) are simplified by combining $[\text{m}^2]$ and [kg] into a single composite dimension, resulting in M=2 dimensions. A matrix transform technique is used to

Table 1 Dimensional set matrix

	Desired parameters	Repeating parameters
Dimensions	B_{D}	A_{D}
π- groups	I	C_{π}

choose the variables, the dimensions, and the dimensionless pi-groups. These elements can be represented in matrix form, as shown in Table 1, where A_{D} is the square and the full rank matrix and B_{D} is the desired variable dimensional matrix. The matrix C_{π} can be calculated from (10).

$$C_{\pi} = -(A_{\mathrm{D}}^{T}.B_{\mathrm{D}})^{T} \tag{10}$$

The matrices shown in Table 2 enable the formation of pi-groups, thus obtaining the scaling factors by equating the relevant pi-groups of the motor operating points ($\pi_{\mathrm{k,mop}}$). The method of scaling the desired variables of the given operating point is shown in (11) and (12).

$$\pi_{1,\mathrm{mop,m}} = \pi_{1,\mathrm{mop,v}} \Longrightarrow \quad \frac{T_{\mathrm{m}}}{T_{\mathrm{max.m}}} = \frac{T_{\mathrm{v}}}{T_{\mathrm{max.v}}} \quad \Longrightarrow \quad T_{\mathrm{m}} = T_{\mathrm{v}}\frac{T_{\mathrm{max.m}}}{T_{\mathrm{max.v}}} \tag{11}$$

$$\pi_{2,\mathrm{mop,m}} = \pi_{2,\mathrm{mop,v}} \Longrightarrow \frac{\Omega_{\mathrm{m}}T_{\mathrm{max.m}}}{P_{\mathrm{max.m}}} = \frac{\Omega_{\mathrm{v}}T_{\mathrm{max.v}}}{P_{\mathrm{max.v}}} \Longrightarrow \quad \Omega_{\mathrm{m}} = \Omega_{\mathrm{v}}\frac{T_{\mathrm{max.v}}P_{\mathrm{max.m}}}{T_{\mathrm{max.m}}P_{\mathrm{max.v}}} \tag{12}$$

3.2 Drive Cycles

To down-scale the real drive cycle, the original driving cycle undergoes adjustments using specific coefficients: the speed coefficient C_{Ω}, the time difference coefficient $C_{\Delta \mathrm{t}}$, and the torque coefficient C_{T} as given in (13), (14), and (15). In this proposed method, the torque and the speed coefficients are derived from the dimensionless method, while the time difference coefficient is calculated based on the quasi-static model and considering the dominance of the accelerating torque [17]. The flowchart of the overall down-scaling process is shown in Fig. 3.

$$\Omega_{\mathrm{m}} = \Omega_{\mathrm{v}}\frac{T_{\mathrm{max.v}}P_{\mathrm{max.m}}}{T_{\mathrm{max.m}}P_{\mathrm{max.v}}} \Longrightarrow \quad C_{\Omega} = \frac{T_{\mathrm{max.v}}P_{\mathrm{max.m}}}{T_{\mathrm{max.m}}P_{\mathrm{max.v}}} \tag{13}$$

$$T_{\mathrm{m}} = T_{\mathrm{v}}\frac{T_{\mathrm{max.m}}}{T_{\mathrm{max.v}}} \Longrightarrow \quad C_{\mathrm{T}} = \frac{T_{\mathrm{max.m}}}{T_{\mathrm{max.v}}} \tag{14}$$

$$C_{\mathrm{T}}.a = \frac{C_{\Omega}\Delta v}{C_{\Delta t}\Delta t} \Longrightarrow \quad C_{\Delta t} = \frac{C_{\Omega}}{C_{\mathrm{T}}} \tag{15}$$

Table 2 Motor operating point model dimensional set matrix

	T	Ω	T_{max}	P_{max}
$\mathrm{m^2kg}$	1	0	1	1
s	-2	-1	-2	-3
$\pi_{1,\mathrm{mop}}$	1	0	-1	0
$\pi_{2,\mathrm{mop}}$	0	1	1	-1

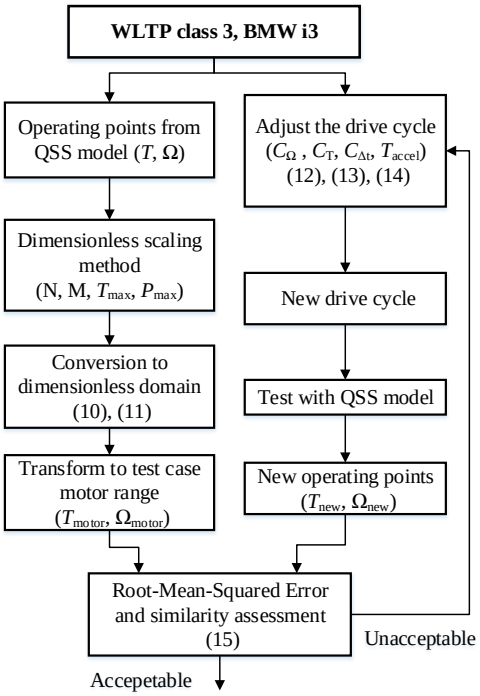

Fig. 3: Flowchart of the proposed down-scaling method.

The down-scaled drive cycles can then be employed as input for the test case motors in the laboratory. This utilization enables the derivation of new torque-speed operating points by incorporating the corrected drive cycles into the quasi-static model. These new operating points are then compared to the operating points obtained using the dimensionless method. This comparison allows for the analysis of similarity between the two sets of operating points, providing insights into the effectiveness of the proposed down-scaling approach.

4 Selected Case Study Examples

For the investigation of the proposed method, three test case speed-over-time drive cycles were chosen from the field of traction electrification that are most demanding with respect to different operating points. A total of 18 vehicles was analyzed for characteristics such as size, weight, aerodynamics, performance, and range, from which two vehicles, a mid-range (BMW i3) and a small range (Smart EQ) passenger car, were selected for the study. To experimentally study the drive cycles, two test case machines are available in the laboratory: An Induction Motor (IM) and a Permanent Magnet Synchronous Motor (PMSM). The vehicles and the lab motors specifications are listed in Table 3. The torque-speed profiles of the motors used in two cars for WLTP class 3, Artemis 130 and Braunschweig City Driving Cycle (BCDC) are obtained by considering the quasi-static longitudinal vehicle model.

5 Results and Discussions

To demonstrate the effectiveness of the proposed down-scaling method, first the operating points of the BMW i3 and Smart EQ motors on WLTP class 3 driving cycle are scaled down to

Table 3 Vehicle and motor specifications [23], [24]

Vehicle Specifications		
Parameters	**Values**	
	BMW i3	**Smart EQ**
Vehicle Mass	1365 kg	1095 kg
Rotating Mass	5%	4%
Vehicle Cross-section	2.6 m^2	2.2 m^2
Wheel Diameter	0.7 m	0.595 m
Drag Coefficient	0.3	0.38
Rolling Friction Coeff.	0.01-0.02	0.01-0.02
Machine Type	PMSM	PMSM
Maximum Torque	250 Nm	160 Nm
Maximum Power	125 kW	60 kW
Base Speed	4800 rpm	3581 rpm
Maximum Speed	11400 rpm	11475 rpm
Gear Ratio	9.74	9.9
Lab Motor Specifications		
Motor	**Parameters**	**Values**
PMSM	Max. Power	70 W
	Max.Torque	0.1 Nm
	Rated Speed	7000 rpm
	Inertia	0.000113 kgm^2
IM	Max. Power	6.22 kW
	Max.Torque	46.5 Nm
	Rated Speed	1430 rpm
	Inertia	00.0195 kgm^2

the dimensionless domain, then transformed to the range of the two test case motors using (11) and (12). Later, these operating points were compared with the operating points obtained with the adjusted drive cycle obtained from the proposed method. An example of a down-scaled WLTP class 3 drive cycle with the proposed method for use with IM is as shown in Fig. 4. Fig. 5 shows the torque-speed operating points of the BMW i3 and Smart EQ vehicle motors with WLTP class 3 drive cycle. Fig. 6 shows the torque-speed operating points of the test-case motors in the laboratory obtained from the proposed method. As it can be seen in Fig. 6, the down-scaled operating points are well within the operating areas of the two test case motors.

The comparison of the torque-speed operating points of the two test case motors with the dimensionless method and the down-scaled method has found that they closely match. To demonstrate this similarity, the Root Mean Square Error (RMSE) of operating points was calculated using (16), where

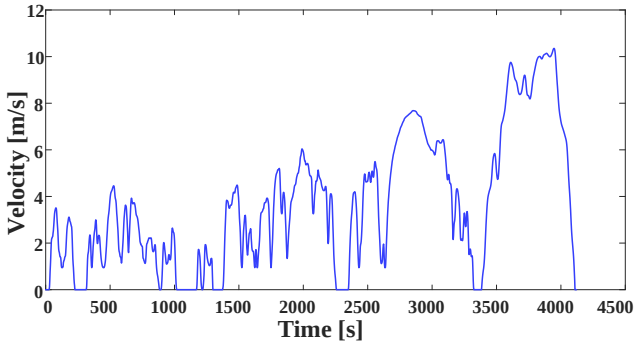

Fig. 4: Example of adjusted WLTP 3 drive cycle for use with the IM in the laboratory.

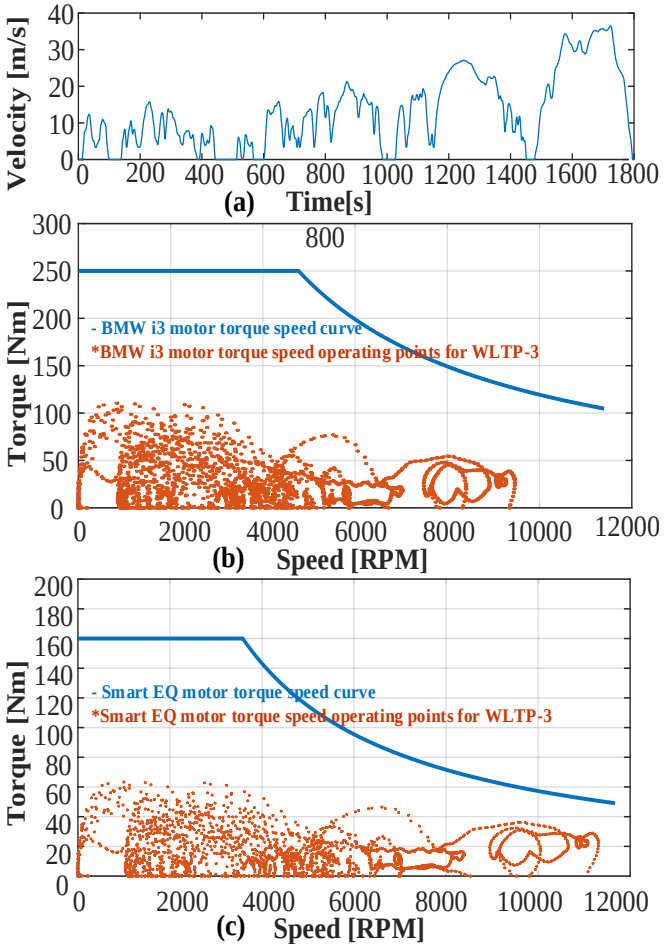

Fig. 5: (a) WLTP class 3 drive cycle (b) BMW i3 torque-speed points in WLTP (c) Smart EQ torque-speed points in WLTP.

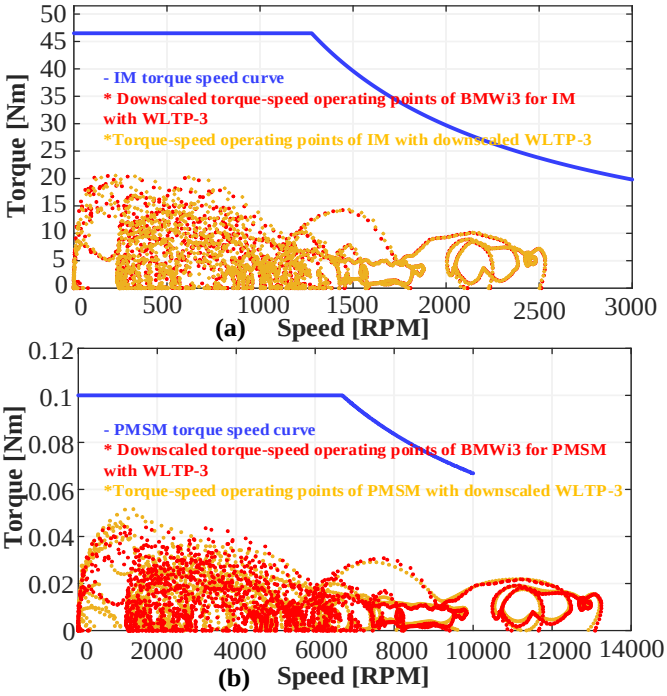

Fig. 6: WLTP class 3 down-scaled T-S profile of BMW i3 (a) for IM (b) for PMSM.

N, m_i and s_i denote the number of data, operating points from the dimensionless domain and operating points obtained from the down-scaled drive cycles respectively.

$$\text{RMS Error } = \sqrt{\frac{\sum_{i=1}^{N} |m_i - s_i|^2}{N}} \tag{16}$$

This error is 1.69 % and 1.41% for the IM and the PMSM example case machines, respectively. Similar comparisons were made for other two drive cycles as shown in Fig. 6. In the case of the PMSM, with the Artemis 130 drive cycle, this error is 0.94% and with BCDC, this error is 2.07%. Similarly, in the case of the IM, with the Artemis 130, this error is 0.86% and with BCDC, it is 1.89%. The down-scaled operating points with reference to Smart EQ motor showed smaller error in contrast to that with BMW i3 motor. These numbers indicate that the proposed drive cycle down-scaling method for use case with lab motors is highly effective.

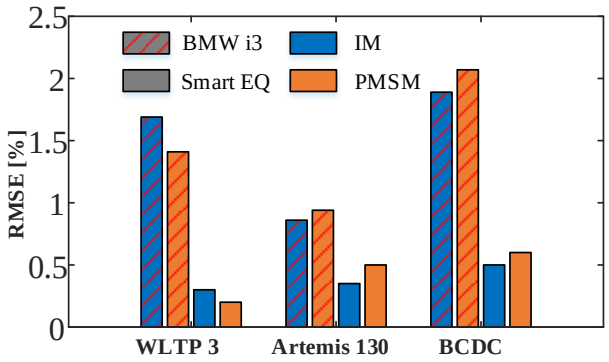

Fig. 7: RMSE of operating points of PMSM and IM originating from two different vehicle motors with down-scaling method.

6 Conclusion

This work presents a methodology for down-scaling the drive cycles of electric vehicles for their use cases in the given laboratory motors whose ratings and ranges are typically smaller. The use cases are presented by means of two laboratory test case machines, a PMSM and an IM. A baseline is established using a medium and a small range car on the demanding drive cycles from the traction applications. First the operating points of the test case motors are determined by the down-scaling method in the dimensionless domain. The effectiveness of the proposed method is shown by comparing the operating points after down-scaling the drive cycle.

Overall, this work provides a valuable methodology for down-scaling drive cycles in electric vehicles, with promising applications for enhancing the efficiency and performance of electric vehicle systems.

7 Acknowledgements

This work is supported by the joint DFG/FWF Collaborative Research Centre CREATOR (CRC – TRR361/F90) at TU Darmstadt, TU Graz and JKU Linz.

8 References

[1] S. G. Selvakumar, ‘Electric and Hybrid Vehicles – A Comprehensive Overview’, in 2021 IEEE 2nd International Conference On Electrical Power and Energy Systems (ICEPES), Dec. 2021, pp. 1–6. doi: 10.1109/ICEPES52894.2021.9699557.

[2] E. A. Grunditz, T. Thiringer, and N. Saadat, ‘Acceleration, Drive Cycle Efficiency, and Cost Tradeoffs for Scaled Electric Vehicle Drive System’, IEEE Trans. Ind. Appl., vol. 56, no. 3, pp. 3020–3033, May 2020, doi: 10.1109/TIA.2020.2976861.

[3] E. Agamloh, A. von Jouanne, and A. Yokochi, ‘An Overview of Electric Machine Trends in Modern Electric Vehicles’, Machines, vol. 8, no. 2, p. 20, Apr. 2020, doi: 10.3390/machines8020020.

[4] L. D. D. Harvey, ‘Cost and energy performance of advanced light duty vehicles: Implications for standards and subsidies’, Energy Policy, vol. 114, pp. 1–12, Mar. 2018, doi: 10.1016/j.enpol.2017.11.063.

[5] S. Kamguia Simeu and N. Kim, ‘Standard Driving Cycles Comparison (IEA) & Impacts on the Ownership Cost’, in WCX World Congress Experience, Apr. 2018. doi: https://doi.org/10.4271/2018-01-0423.

[6] L. Guzzella and A. Amstutz, ‘The QSS Toolbox Manual’. Jun. 2005. Available: https://idsc.ethz.ch/research-guzzella-onder/downloads.html

[7] C. Paar and A. Muetze, ‘Influence of Dry Clutch and ICE Transmission Integration on the Thermal Load of a PM-Based Integrated Starter-Generator’, IEEE Trans. Transp. Electrification, vol. 3, no. 3, pp. 716–723, Sep. 2017, doi: 10.1109/TTE.2017.2688185.

[8] G. Gagliardi, A. Casavola, W. Nesci, and G. Prodi, A quasi-static simulation tool for the design and optimization of hybrid powertrains. 2012.

[9] L. Dang, N. Bernard, N. Bracikowski, and G. Berthiau, ‘Design Optimization with Flux Weakening of High-Speed PMSM for Electrical Vehicle Considering the Driving Cycle’, IEEE Trans. Ind. Electron., vol. 64, no. 12, pp. 9834–9843, Dec. 2017, doi: 10.1109/TIE.2017.2726962.

[10] Q. Li, T. Fan, X. Wen, Y. Li, Z. Wang, and J. Guo, ‘Design optimization of interior permanent magnet sychronous machines for traction application over a given driving cycle’, in IECON 2017 - 43rd Annual Conference of the IEEE Industrial Electronics Society, Beijing, Oct. 2017, pp. 1900–1904. doi: 10.1109/IECON.2017.8216321.

[11] A. Fatemi, N. A. O. Demerdash, T. W. Nehl, and D. M. Ionel, ‘Large-Scale Design Optimization of PM Machines Over a Target Operating Cycle’, IEEE Trans. Ind. Appl., vol. 52, no. 5, pp. 3772–3782, Sep. 2016, doi: 10.1109/TIA.2016.2563383.

[12] S. Pastellides, S. Gerber, R.-J. Wang, and M. Kamper, ‘Evaluation of Drive Cycle-Based Traction Motor Design Strategies Using Gradient Optimisation’, Energies, vol. 15, no. 3, p. 1095, Feb. 2022, doi: 10.3390/en15031095.

[13] V. T. Buyukdegirmenci, A. M. Bazzi, and P. T. Krein, 'Evaluation of Induction and Permanent-Magnet Synchronous Machines Using Drive-Cycle Energy and Loss Minimization in Traction Applications', IEEE Trans. Ind. Appl., vol. 50, no. 1, pp. 395–403, Jan. 2014, doi: 10.1109/TIA.2013.2266352.

[14] S. Kalt, S. Wolff, and M. Lienkamp, 'Impact of Electric Machine Design Parameters and Loss Types on Driving Cycle Efficiency', in 2019 8th International Conference on Power Science and Engineering (ICPSE), Dublin, Ireland, Dec. 2019, pp. 6–12. doi: 10.1109/ICPSE49633.2019.9041132.

[15] S. P. Emami, E. Roshandel, A. Mahmoudi, and S. Khaourzade, 'IPM Motor Optimization for Electric Vehicles Considering Driving Cycles', in 2021 31st Australasian Universities Power Engineering Conference (AUPEC), Perth, Australia, Sep. 2021, pp. 1–5. doi: 10.1109/AUPEC52110.2021.9597815.

[16] M. Salameh, I. P. Brown, and M. Krishnamurthy, 'Driving Cycle Analysis Methods Using Data Clustering for Machine Design Optimization', in 2019 IEEE Transportation Electrification Conference and Expo (ITEC), Detroit, MI, USA, Jun. 2019, pp. 1–6. doi: 10.1109/ITEC.2019.8790523.

[17] T. Huynh and M.-F. Hsieh, 'Performance Analysis of Permanent Magnet Motors for Electric Vehicles (EV) Traction Considering Driving Cycles', Energies, vol. 11, no. 6, p. 1385, May 2018, doi: 10.3390/en11061385.

[18] A. R. Tariq, C. E. Nino-Baron, and E. G. Strangas, 'Design and analysis of PMSMs for HEVs based upon average driving cycle efficiency', in 2011 IEEE International Electric Machines & Drives Conference (IEMDC), Niagara Falls, ON, Canada, May 2011, pp. 218–223. doi: 10.1109/IEMDC.2011.5994849.

[19] T. D. Gillespie, Fundamentals of Vehicle Dynamics. Society of Automotive Engineers, 1992.

[20] E. Buckingham, 'On physically similar systems; illustrations of the use of dimensional equations', Phys. Rev., vol. 4, no. 4, p. 345, 1914.

[21] T. Szirtes, Applied dimensional analysis and modeling. Butterworth-Heinemann, 2007.

[22] M. D. Petersheim and S. N. Brennan, 'Scaling of hybrid-electric vehicle powertrain components for Hardware-in-the-loop simulation', Mechatronics, vol. 19, no. 7, pp. 1078–1090, Oct. 2009, doi: 10.1016/j.mechatronics.2009.08.001.

[23] 'Technical Data BMW i3 (120Ah)', https://www.press.bmwgroup.com/global/article/detail/T0148284EN/the-bmw-i3?language=en, accessed Jan. 09, 2023.

[24] 'Smart EQ fortwo coupe', EV Database, https://ev-database.org/car/1230/Smart-EQ-fortwo-coupe, accessed Jan. 09, 2023.